Nanocarbon Synthesis

DOI: 10.1002/anie.201200969

Spherical Structures Composed of Multiwalled Carbon Nanotubes: Formation Mechanism and Catalytic Performance**

Jian Zhang, Rui Wang, Enze Liu, Xufeng Gao, Zhenhua Sun, Feng-Shou Xiao, Frank Girgsdies, and Dang Sheng Su**

The chemical-vapor-deposition (CVD) process is sufficiently well developed to allow the large-scale production of carbon nanotubes (CNTs).[1] Metal nanoparticles (Fe, Co, Ni, etc.), which are usually immobilized on a solid support, decompose the gaseous hydrocarbon feedstocks into fragmented carbon units at elevated temperatures of 700–1100 °C. The metal carbides formed serve as a structural template for the growth of filamentous carbon.[2,3] The produced CNTs are not firmly attached to the inert support and are thus inevitably detached, in particular during liquid-phase purification or mechanical treatment.[4] The biggest difficulties in handling the loose powder are presented by filtration steps in the slurry-phase operations and the large drops in pressure in fixed-bed reactors. These problems very much limit the application of CNTs on a large scale. The fabrication of carbon filaments on a structured support (e.g., activated carbon, carbon fibers, porous frameworks, graphite)[5,6] has also suffered from discontinuities in the structure. The future use of CNTs has also been restricted by the technical requirements and the necessary high energy consumption of the complicated CVD process.

To avoid mechanical post-treatment of CNT powder and the risk of explosion during CVD synthesis, we have explored a simple method to produce monolithic CNTs directly as millimeter-scale spheres, featuring an integral continuity in the structure from the microscopic to the macroscopic scale. The whole process of CNT growth has been conducted in a flow of ultrapure N_2, involving a set of elementary steps in the solid phase which are less complex than the widely used CVD process. The growth of CNTs is based on a solid-phase reaction and well-graphitized nanotubes can be obtained even at temperatures as low as 400 °C. All growth events were observed directly by in situ transmission electron microscopy (TEM), X-ray diffraction (XRD), IR and Raman spectroscopy, and thermogravimetric analysis.

A commercial styrene–divinylbenzene copolymer resin was used as the carbon precursor. According to Scheme 1, the ion-exchanged resin spheres were calcined at 800 °C in a flow of N_2 or under vacuum, after which the average diameter decreased from 0.77 to 0.49 mm, while the bulk density increased from 0.55 to 0.91 g mL^{-1}. A novel macroscopic structure can be clearly seen, especially after the Fe nanoparticles and the amorphous carbon species had been removed by heating the spheres in concentrated HNO_3 at reflux. As seen in Figure 1a, the twisted nanotubes construct a monolith which maintains a spherical shape. In the cross-sectional views of the manually crushed spheres there is no difference in structure between the bulk and the surface, indicating a homogeneous distribution of the nanotubes in the millimeter-scale spheres (Figure 1b). The nitrogen adsorption/desorption isotherm shows a hysteresis loop, which is a typical feature of a typical mesoporous structure. The measured BET surface area and the pore volume are 223.7 m^2 g^{-1} and 0.42 mL g^{-1}, respectively. The distribution of the pores ranges between about 2 and 15 nm.

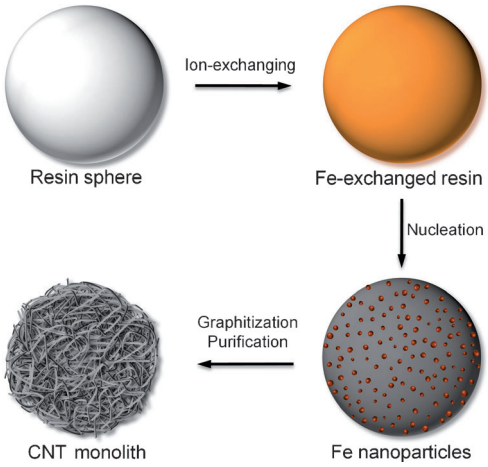

Scheme 1. Schematic representation of the synthesis of CNT monoliths.

The high-resolution SEM images in Figure 1a show that the produced CNTs are mostly open-ended and the inner

[*] Prof. Dr. J. Zhang, Dr. R. Wang, X. F. Gao, Dr. Z. H. Sun, Prof. Dr. D. S. Su
Shenyang National Laboratory for Materials Science
Institute of Metal Research, Chinese Academy of Sciences
Shenyang, 110016 (China)
E-mail: dssu@imr.ac.cn
Dr. F. Girgsdies, Prof. Dr. D. S. Su
Department of Inorganic Chemistry
Fritz Haber Institute of the Max Planck Society
14195 Berlin (Germany)
Prof. F. S. Xiao
Department of Chemistry, Zhejiang University
Hangzhou 310027 (China)
E-mail: fsxiao@zju.edu.cn

[**] This work was supported financially by MOST (2011CBA00504), NSFC (21133010, 21103203, 50921004, 20973079), Institute of Metal Research (O9NBA111A1), Liaoning Province (20101121), Max Planck Society (Enerchem), and Zhejiang University. We gratefully acknowledge Dr. Di Wang, Jinwei Li, Hao Zhang, Ming Xin, Dr. Bo Zhu, and Prof. Feng Li for technical assistance and BESSY for supporting XPS measurements.

Supporting information for this article is available on the WWW under http://dx.doi.org/10.1002/anie.201200969.

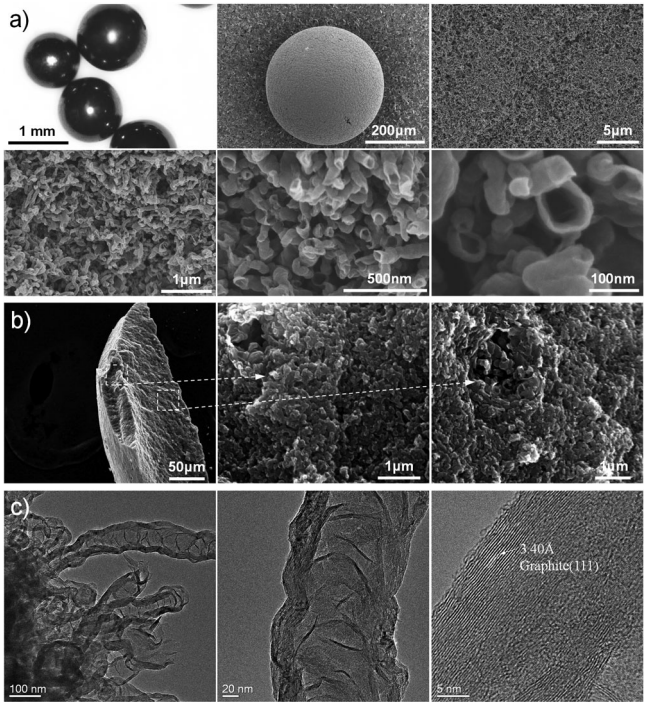

Figure 1. Microscopic images of purified CNT spheres calcined at 800 °C. a) Optical microscopy and SEM images at various magnification scales. b) SEM images of crushed sections of purified CNT spheres. c) TEM and HRTEM images of individual CNTs.

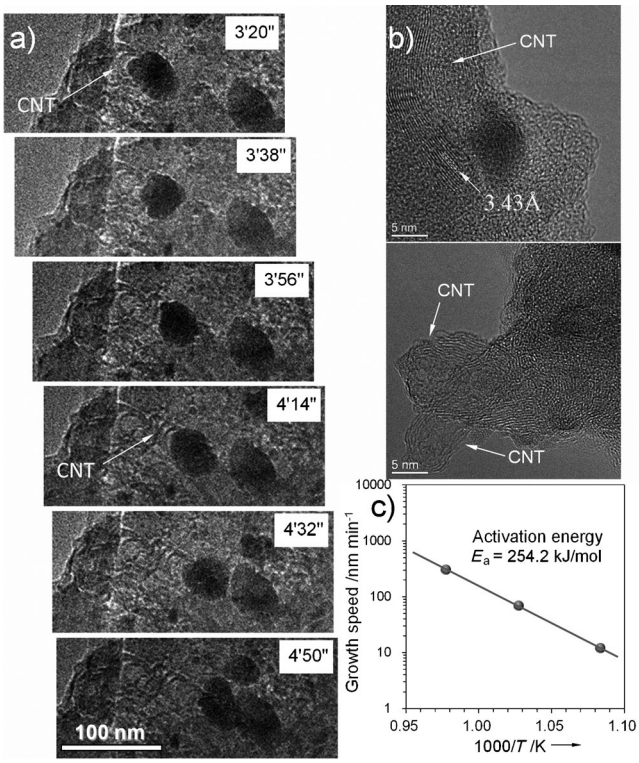

Figure 2. Characterization of CNT growth by a solid-phase process. a) Time-dependent in situ TEM images at 700 °C. b) Ex situ high-resolution TEM images of iron carbide nanoparticles and carbon nanotubes that were synthesized at 400 °C. c) Growth speed of CNTs as a function of the inverse absolute temperature.

diameter of the tubes ranges from 60 to 90 nm. Some thin graphitic pieces can be clearly observed as the herringbone patterns on the inner walls (Figure 1c). The majority of the tubes are not fully blocked by such dangling graphitic kinks but retain the open features of the inner channels. The abundance of microscopic defects inside the channels permits the tight binding of external materials such as metal nanoparticles, proteins, and drugs. The HRTEM images show that the sheath body is highly graphitized and durable. A microforce compressive test shows that the spheres can withstand a maximum load of 17.6 ± 7.2 N, a crushing force more than 11 times higher than that for the nanostructure-free resin spheres that were carbonized under the same conditions, except that oxalate salts were used during the ion-exchange treatment. This is a result of the special characteristics of the self-supported nanostructure of the monolithic CNTs.

We used in situ microscopic and spectroscopic techniques to investigate the formation mechanism of the CNTs by a solid-phase route. The in situ TEM experiments were carried out at temperatures of 400–800 °C using heating stages. Figure 2a highlights the sequence of CNT formation at 700 °C, when the growth rate is approximately 69 nm min^{-1}. An iron-based nanoparticle fluctuates inside the solid and simultaneously catalyzes the steady growth of one bamboo-like nanotube with an outer diameter of around 37 nm. According to the XRD (Figure 3a) and electron diffraction patterns, the nanoparticles remain predominantly solid or fluctuating crystalline throughout the whole process. The dynamic reshaping of the metal crystals makes it possible for them to creep under the barrier of the surrounding carbon solid, leading to the self-supported and porous structure of the

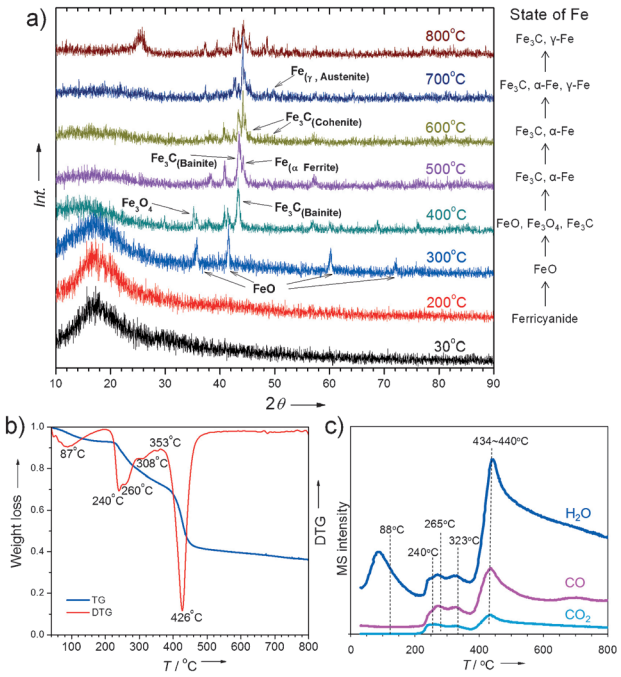

Figure 3. a) In situ powder XRD patterns along with the synthesis route up to 800 °C. Thermal analysis (b) and mass spectra (c) during TG-DSC experiments with a mass spectrometer to monitor the product mixture in the effluent. Conditions: heating rate 5 °C min^{-1}, Ar 40 mL min^{-1}. In (a) the traces are offset vertically for clarity.

produced spheres. We were delighted to observe graphitized nanotubes at temperatures as low as 400 °C. Figure 2b shows the morphology of a sample that was calcined at 400 °C for 4 h. The average outer diameter of the produced nanotubes ranged between 7 and 13 nm. The lattice spacing of 3.43 Å indicates that the (002) plane of graphite is the sheath. The sharp lattice fringes suggest a certain degree of crystallinity, which is very exciting because the solid-phase process produces graphitized nanofilaments only at temperatures above 750 °C according to the available literature.[7]

When the temperature was increased from 650 to 750 °C, the estimated growth speed increased from 12 to 305 nm min^{-1}. The Arrhenius plot of the speed against the inverse absolute temperature suggests an activation energy of 254.6 kJ mol^{-1} for this process (Figure 2c), which is around 30–80 kJ mol^{-1} higher than that of the CVD route.[12] More details can be found in Movies S1 in the Supporting Information, which illustrates one sequence of CNT growth at 700 °C. We can clearly see the movements of the Fe-based nanoparticles, including nucleation, agglomeration, redistribution, and fluctuation.

Comprehensive in situ characterization using XRD, DRIFT, and Raman spectroscopy made it possible to understand the crystalline state of the nanoparticles as well as the bonding state of the polymeric carbon atoms, which we believe are the key to our synthesis strategy. As shown in Figure 3a, the transformation of the Fe-based components takes place in three stages, from room temperature to 800 °C. A few ferricyanide ions, as the precursor, are partially converted into FeO between 200 and 300 °C (stage 1), probably assisted by the large quantity of oxygen species such as the hydroxy groups in the resin. The thermal treatment was monitored by thermogravimetric analyses as part of the temperature-programmed desorption. As seen in Figure 3b, the weight loss of 21 % at 300 °C can be primarily attributed to H_2O desorption below 200 °C. The peaks of the released CO, CO_2, and H_2O at 240 °C and 265 °C suggest that the formation of FeO is accompanied by the oxidation of the polymer-type carbon.

A further increase in the temperature transforms the FeO into Fe_3C and Fe_3O_4 (stage 2), during which time the weight of the sample decreases by 11 % to release abundant CO, CO_2, and H_2O, peaking at 434–440 °C (Figure 3c). The pronounced diffraction peak of the Fe_3C phase, which has been reported to catalyze the growth of CNTs during the CVD process,[2,3] therefore makes us believe that the formation of CNTs takes place at a temperature as low as 400 °C. The patterns of oxides completely disappear as the temperature reaches 500 °C, leaving only metallic Fe and Fe_3C. The third stage, ranging from 500 to 800 °C, mainly involves the phase transformation of Fe_3C (bainite→cohenite), and metallic Fe (ferrite (α)→austenite (γ)). At 800 °C, the crystalline forms include only austenite, cohenite, and graphite.

Fourier transform infrared spectroscopy helped us to identify the change in chemical bonding during the heating procedures (Figure 4a). The fresh sample displays all the features of the styrene–divinylbenzene copolymer and ferricyanide. The wide band ranging from 3300 to 3600 cm^{-1} corresponds to the hydroxy stretching vibrations, while the

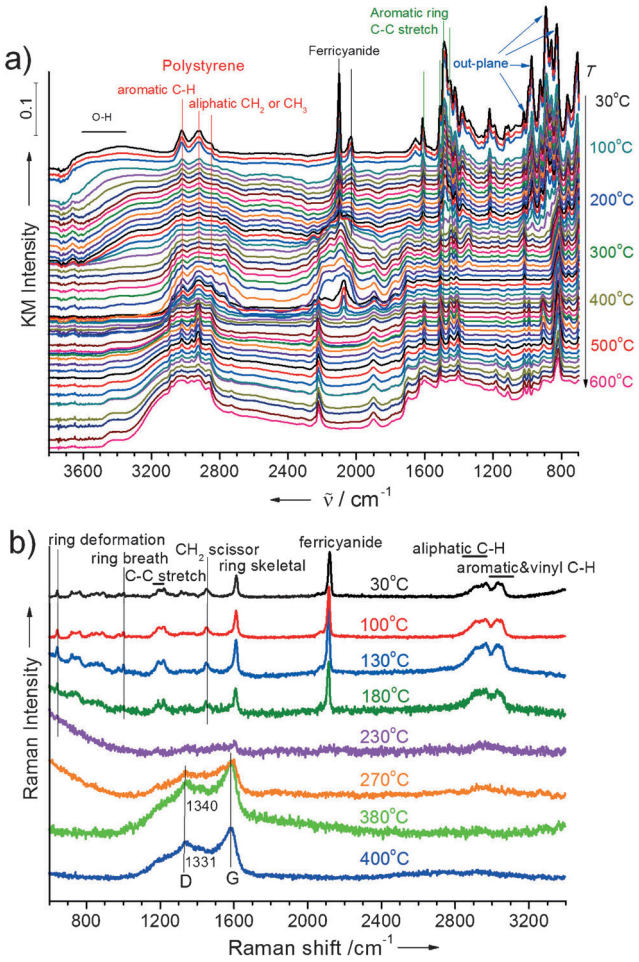

Figure 4. Spectroscopic in situ analysis of CNT growth from the ferricyanide-exchanged resin powder that was heated inside the in situ cells. a) DRIFT patterns ranging from 30 to 600 °C. b) Raman patterns ranging from 30 to 400 °C.

lower ones at 3020 and 2923 cm^{-1} are attributed to the asymmetric vibrations of the aromatic ring and the aliphatic C–H bonds in the polymer matrix, respectively.[13] As the temperature was increased up to 260 °C, a gradual attenuation and the final disappearance of the three important components were observed: ferricyanide as the Fe precursor (2101 and 2030 cm^{-1}), substituted phenyl rings in the polymer matrix (1611, 1511, 1487, and 1458 cm^{-1}), and the aromatic ring C–H bonds in the polymer matrix (1019, 975, 890 and 827 cm^{-1}).[14,15] Based on the appearance of the FeO crystals at 300 °C (Figure 3a) we therefore conclude that in stage 1, the nucleation of FeO takes place and simultaneously the cross-linked polymer framework is destroyed. The latter comprises the scission of C–C and C–H bonds in both the aliphatic and phenyl units with the release of CO, CO_2, and H_2O.

In situ Raman tests confirmed the disappearance of the aromatic and aliphatic C–H stretching (2900–3100 cm^{-1}), and the benzene skeletal stretching (1583–1613 cm^{-1}) modes[16] at around 270 °C (Figure 4b). The process of carbonization was clearly observed at 380 °C, as shown by the *D* and *G* bands at 1340 cm^{-1} and 1583 cm^{-1}, respectively. The *D* band shifted

downwards at 1331 cm^{-1} as the temperature reached 400 °C, indicating an enhanced domain size of the graphitic structure and a decreased amount of amorphous carbon.[17] This phenomenon can be related to the catalytic growth of the CNT structure in this temperature region (Figure 2b).

In our case, the forms of iron are ferricyanide ions, ferrous oxide, iron carbide, and metallic iron. The temperature triggers the migration of the ferricyanide ions to destroy their bonding with the polymer matrix. As the temperature reached 260 °C, the ionic iron components disappear, while the nucleation into ferrous oxide becomes extremely significant. Ferricyanide ions probably oxidize the surrounding polymeric carbon into CO and CO_2, along with the reduction of Fe^{III} to Fe^{II} to form the ferrous oxide nanocrystals. Later, at 400 °C, the Fe–C interaction becomes more intense and induces the disproportionation of Fe^{II} into Fe_3O_4 and Fe_3C, decreasing the sample weight by around 25% to release significant amounts of CO, CO_2, and H_2O. A further increase in the temperature leads to the fluctuating carbide nanoparticles and the templated growth of CNTs in large quantities. The extensive diffusion of carbide nanoparticles finally converts the polymer sphere into a porous CNT framework at 800 °C.

The chemical composition of the CNT surface and the functional groups of the purified CNT monoliths were detailed by using synchrotron-excited X-ray photoelectron spectroscopy (XPS). Only the elements carbon and oxygen can be identified on the surface of the purified sample (Figure 5a). Most of the iron was removed when the sample was heated in HNO_3 at reflux, and analysis by atomic adsorption indicated an Fe content of only 0.2 wt%. The residual Fe atoms are likely embedded within the graphitic framework, since we did not observe an Fe signal in the XPS spectra. We were surprised to find that the oxygen content is as high as 23.2%; carbonyl oxygen atoms, which give rise to a peak at 531.6 eV, account for 10.1%. We could reasonably expect satisfactory catalytic activity on a CNT monolith featuring a large amount of active oxygen atoms and an open macroscopic structure.

Oxygen functional groups are known to terminate the deficient sites in CNTs such as edges and structural defects. Since the surface and structure of CNTs can be controlled much more readily than the surface features of metal catalysts, CNTs may potentially display superior performance. In addition, CNTs display high activity, and are free of coke and environmentally benign.[18–22] However, the reaction is always performed in a fixed-bed reactor and the use of fine powders results in a hot spot as well as a pressure drop. The use of a bulky, monolithic catalyst that is free of a pressure drop, such as a spherical monolith, is very desirable. The catalytic performance of the CNT monolith spheres was evaluated for the oxidative dehydrogenation of ethylbenzene. Figure 5b shows the outstanding performance of the CNT monolith at 400 °C. Its activity is similar to that of commercial CNT powder, providing almost the same styrene yield, while the monolith displays superior selectivity of around 90%. In comparison, the pure CNT powder gives a value of only 68%. Figure 5c illustrates the conversion–selectivity relationship that is normally used to describe the

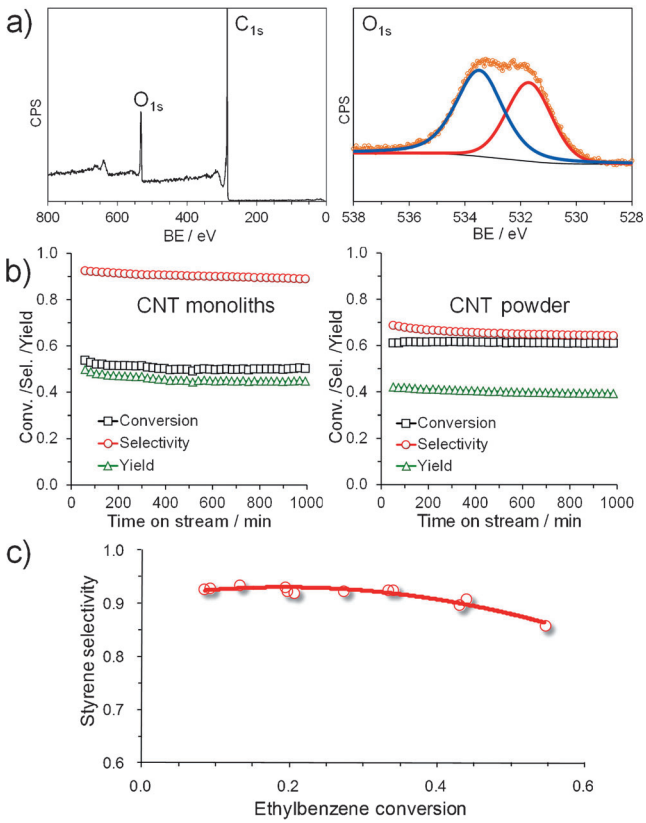

Figure 5. Characterization and catalysis evaluation of purified CNT spheres. a) Survey and O1s XPS spectra of purified CNT monoliths. b) Time-on-stream profiles of ethylbenzene conversion, styrene selectivity, and yield. c) Conversion–selectivity profiles. Reaction conditions: 100 mg sample, 400 °C, 2.9% ethylbenzene, 7.2% O_2, He as balance, total flow rate 10 mL min^{-1}.

capability of a single catalysis material. The selectivity of the unsaturated product is known to show an inverse proportional dependence on the conversion of the alkane. For the CNT monolith, the selectivity remains as high as 87%, even at a conversion of 55%. This can be related to the advantage of the monolithic structure in allowing the immediate diffusion of the styrene product.[23] Moreover, the ODH process, as an alternative to direct dehydrogenation (DH), has been limited by its low selectivity and the safety issues relating to the handling of combustive reactants. The CNT monolith is much more selective than the reported ODH catalyst, and reaches a selectivity close to that of the DH reaction (93–97%). Both the spherical architecture and tubular nanostructure remain intact after heating in HNO_3 at reflux and after the oxidative dehydrogenation reaction. Note that the ODH process based on the CNT monolith is much more energy-saving than the industrial DH process which is performed at around 630 °C with the cycling of excess steam as the protection agent.

We have shown that the graphitization of an ion-exchanged resin can produce structured CNTs directly in a solid-phase process and we have described the detailed changes taking place among the iron and carbon species at elevated temperatures. The growth of the tubular carbon goes through a series of stages, including the nucleation of iron oxides, their reaction with the polymer framework, the

formation of iron carbide, the catalytic growth of graphitic tubes and, finally, the production of monolithic CNTs. The solid-phase growth events greatly differ from our present knowledge about chemical-vapor-deposition processes, providing a more complete understanding of the metal–carbon interactions governing the formation of a carbon nanostructure.[24] This simple methodology, based on widely available chemical feedstocks, should promote the large-scale production of CNTs and the associated applications of CNTs in the near future.

Experimental Section

Potassium ferricyanide (0.5 g) was dissolved in 25 mL of ultrapure water to form a transparent solution. Styrene–divinylbenzene copolymer resin spheres (4 g) were immersed into the solution. The ion-exchanged resin was then washed by ultrapure water to remove the weakly adsorbed ions. After drying overnight, the spheres were put inside a tube furnace for heat treatment. In a flow of ultrapure N_2 (99.995%), the temperature was increased to 400–800 °C and held for 4 h. After the system was cooled down to room temperature, the calcined spheres were taken out of the furnace. The residual Fe can be efficiently removed by refluxing in 160 mL of concentrated HNO_3 solution (65%) at 120 °C. The mixture was filtered, fully washed with deionized water, and dried at 80 °C under air overnight. The resulting solid was the purified CNT monoliths used in subsequent tests.

Structural properties (specific surface area, pore size, etc.) were determined by N_2 physisorption at −196 °C on a Micrometrics ASAP 2020 instrument. In situ TEM was performed with a Philips CM200 FEG electron microscope operating at 200 kV, equipped with a Gatan Tridiem imaging filter and a sample holder resistant up to 1000 °C. The sample was dispersed on a Cu grid and heated to a high temperature by increasing stepwise the current through the heating filament. Low-dose electron-beam imaging was used to prevent sample damage and additional heating effects of the electron beam. One image per three seconds was recorded using the serial imaging mode and all the images were used to make the video. SEM was conducted using a Hitachi S4800 electron microscope operating at 3–15 kV, equipped with an EDAX detector. The XPS experiments were carried out at the ISISS beamline in the BESSY synchrotron facility at the end station of the FHI-MPG.

In situ powder XRD experiments were performed on a STOE diffractometer ($Cu_{K\alpha}$ radiation, $\lambda = 1.5418$ Å) in Bragg–Brentano geometry equipped with a secondary monochromator and a scintillation counter. The sample was heated to the target temperature in a flow of helium, controlled by a mass-flow controller. In situ diffuse reflectance infrared Fourier transform (DRIFT) experiments were conducted on a Thermo Nicolet iS10 infrared spectroscope equipped with a Spectra-Tech Collector II cell and connected with an AVI Omnistar 200 mass spectrometer. In situ Raman measurements were made using a Thermo Scientific DXR Raman Microscope with a 532 nm laser (50 s exposure time and 50 μm slit aperture). All the Raman spectra were recorded in a N_2 flow (50 mL min^{-1}) by heating from room temperature up to 400 °C.

The oxidative dehydrogenation of ethylbenzene was carried out at 400 °C in a quartz-plug flow reactor with 100 mg of purified CNT monoliths. For comparison, one commercial CNT sample (Baytubes, Bayer Materials) was also treated with concentrated HNO_3 and tested in the ODH reaction under the same conditions. A stream of the reactant (10 mL min^{-1}, 1 atm, $C_8H_{12}\% = 2.9\%$, $O_2\% = 7.2\%$) was then fed to the reactor from a liquid saturator using He as the carrier gas. The reaction products were analyzed with a Varian CP-3800 gas chromatograph equipped with a flame-ionization detector for hydrocarbons and a thermal conductivity detector for the inorganic components.

Received: February 4, 2012
Revised: March 29, 2012
Published online: June 13, 2012

Keywords: carbon nanotubes · heterogeneous catalysis · monoliths · oxidative dehydrogenation · solid-phase synthesis

[1] a) Ç. Öncel, Y. Yürüm, *Fullerenes Nanotubes Carbon Nanostruct.* **2006**, *14*, 17–37; b) J.-P. Tessonnier, D. S. Su, *ChemSusChem* **2011**, *4*, 824–847; c) Q. Zhang, J.-Q. Huang, M.-Q. Zhao, W.-Z. Qian, F. Wei, *ChemSusChem* **2011**, *4*, 864–889.
[2] H. Yoshida, S. Takeda, T. Uchiyama, H. Kohno, Y. Homma, *Nano Lett.* **2008**, *8*, 2082–2086.
[3] R. Sharma, E. Moore, P. Rez, M. M. J. Treacy, *Nano Lett.* **2009**, *9*, 689–694.
[4] M. Endo, K. Takeuchi, Y. A. Kim, K. C. Park, T. Ichiki, T. Hayashi, T. Fukuyo, S. Iinou, D. S. Su, M. Terrones, M. S. Dresselhaus, *ChemSusChem* **2008**, *1*, 820–822.
[5] D. S. Su, X. Chen, G. Weinberg, A. Klein-Hofmann, O. Timpe, S. B. A. Hamid, R. Schlögl, *Angew. Chem.* **2005**, *117*, 5624–5628; *Angew. Chem. Int. Ed.* **2005**, *44*, 5488–5492.
[6] S. S. Tzeng, K. H. Hung, T. H. Ko, *Carbon* **2006**, *44*, 859–865.
[7] O. P. Krivoruchko, N. I. Maksimova, V. I. Zaikovskii, A. N. Salanov, *Carbon* **2000**, *38*, 1075–1082.
[8] P. J. F. Harris, S. C. Tsang, J. B. Claridge, M. L. H. Green, *J. Chem. Soc. Faraday Trans.* **1994**, *90*, 2799–2802.
[9] D. B. Buchholz, S. P. Doherty, R. P. H. Chang, *Carbon* **2003**, *41*, 1625–1634.
[10] A. A. Setlur, S. P. Doherty, J. Y. Dai, R. P. H. Chang, *Appl. Phys. Lett.* **2000**, *76*, 3008–3010.
[11] R. Sergiienko, E. Shibata, S. Kim, T. Kinota, T. Nakamura, *Carbon* **2009**, *47*, 1056–1065.
[12] M. Pérez-Cabero, E. Romeo, C. Royo, A. Monzón, A. Guerrero-Ruíz, I. Rodríguez-Ramos, *J. Catal.* **2004**, *224*, 197–205.
[13] M. Wawrzkiewicz, Z. Hubicki, *J. Hazard. Mater.* **2009**, *164*, 502–509.
[14] C. M. Pharr, P. R. Griffiths, *Anal. Chem.* **1997**, *69*, 4673–4679.
[15] G. Wronski, S. Pasieczna-Patkowska, Z. Hubicki, *Eur. Phys. J. Special Topics* **2008**, *154*, 377–380.
[16] E. Partouche, S. Margel, *Carbon* **2008**, *46*, 796–805.
[17] J. Schwan, S. Ulrich, V. Batori, H. Ehrhardt, S. R. P. Silva, *J. Appl. Phys.* **1996**, *80*, 440–447.
[18] J. Zhang, X. Liu, R. Blume, A. H. Zhang, R. Schlögl, D. S. Su, *Science* **2008**, *322*, 73–77.
[19] J. Zhang, X. Wang, Q. Su, L. J. Zhi, A. Thomas, X. L. Feng, D. S. Su, R. Schlögl, K. Müllen, *J. Am. Chem. Soc.* **2009**, *131*, 11296–11297.
[20] J. Zhang, D. S. Su, A. H. Zhang, D. Wang, R. Schlögl, C. Hébert, *Angew. Chem.* **2007**, *119*, 7460–7464; *Angew. Chem. Int. Ed.* **2007**, *46*, 7319–7323.
[21] J. Zhang, D. S. Su, R. Blume, R. Schlögl, R. Wang, X. G. Yang, A. Gajović, *Angew. Chem.* **2010**, *122*, 8822–8826; *Angew. Chem. Int. Ed.* **2010**, *49*, 8640–8644.
[22] D. S. Su, J. Zhang, B. Frank, A. Thomas, X. C. Wang, J. Paraknowitsch, R. Schlögl, *ChemSusChem* **2010**, *3*, 169–180.
[23] J. G. Speight, H. Heinemann, *Structured Catalysts and Reactors*, 2nd ed., Taylor & Francis, New York, **2006**.
[24] M. Endo, S. Iijima, M. S. Dresselhaus, *Carbon Nanotubes*, Elsevier, Amsterdam, **1996**.

